Biosensors and Bioelectronics: X 16 (2024) 100438

Contents lists available at ScienceDirect

Biosensors and Bioelectronics: X

journal homepage: www.journals.elsevier.com/biosensors-and-bioelectronics-x

Carbon-stabilized porous silicon biosensor for the ultrasensitive label-free electrochemical detection of bacterial RNA gene fragments

Grace Pei Chin [a,1], Keying Guo [b,c,1], Roshan Vasani [a], Nicolas H. Voelcker [a,d,e,**], Beatriz Prieto-Simón [f,g,*]

[a] Faculty of Pharmacy and Pharmaceutical Sciences, Monash University, Parkville, Melbourne, VIC, 3052, Australia
[b] Biotechnology and Food Engineering, Guangdong Technion-Israel Institute of Technology (GTIIT), Shantou, Guangdong, 515063, China
[c] Faculty of Biotechnology and Food Engineering, Technion-Israel Institute of Technology (IIT), Haifa, 3200003, Israel
[d] Commonwealth Scientific and Industrial Research Organization (CSIRO), Clayton, Melbourne, VIC, 3168, Australia
[e] Melbourne Centre of Nanofabrication, Victorian Node of the Australian National Fabrication Facility, Clayton, Melbourne, VIC, 3168, Australia
[f] Department of Electronic Engineering, Universitat Rovira i Virgili, 43007, Tarragona, Spain
[g] ICREA, Pg. Lluís Companys 23, 08010, Barcelona, Spain

ARTICLE INFO

Keywords:
Porous silicon
Carbon stabilization
Electrochemical RNA sensor
Pore-blockage mechanism
Bacterial 16S rRNA gene fragment detection

ABSTRACT

Herein, we report a carbon-stabilized porous silicon (pSi)-based electrochemical biosensing platform for the label- and amplification-free detection of bacterial 16S rRNA gene fragments that facilitates pan-bacterial detection. The sensing approach combines thermally carbonized pSi (THCpSi) structures as novel porous electrochemical transducers, and a highly sensitive sensing mechanism based on partial blockage of the pores caused by hybridization of 16S rRNA gene fragment to the DNA capture probe immobilized within the pores. Pore blockage upon RNA hybridization was quantified via differential pulse voltammetry as a decrease in the oxidation current of the redox pair ($[Fe(CN)_6]^{3/4-}$) added to the measuring solution. The use of carbon-stabilized pSi to build the biosensor has additional benefits: it favors high density of the immobilized bioreceptors and a large electroactive surface area, both further enhancing the overall sensitivity of the biosensor. The easily adjustable pSi morphology is key to design diagnostic tools fit-for-purpose. By tailoring the pore diameter, pore blockage upon analyte hybridization can be maximized, thus enhancing sensitivity. By tailoring film thickness, the surface area can be adjusted to optimize the amount of immobilized bioreceptors and the electroactive surface area. An excellent sensing performance was achieved by building the biosensor on THCpSi structures featuring a 27 nm pore diameter and a 1.6 μm film thickness, whose external surface was coated with a thin layer of silicon nitride (Si_3N_4), the latter contributing to maximize the pore blockage. The biosensor achieved a limit of detection of 2.3 pM when tested in 5% fetal bovine serum.

1. Introduction

The risk of infectious disease outbreaks has increased over the past decades. In 2016, the World Health Organization (WHO) reported infectious diseases as a direct threat to public health, requiring urgent research attention (Bloom and Cadarette 2019). Early diagnosis of infections is key to improve patient's outcomes and stop infection dissemination. Traditional bacterial culturing cannot provide a timely diagnosis and thus the gold standard used in a clinical setting is the molecular technique polymerase chain reaction (PCR). PCR is often limited to a laboratory setting due to the need of a thermal cycler resulting in costly and bulky instrumentation, and requires complicated processes performed by trained personnel (Yang and Rothman 2004). New diagnostic tools are thus required to accurately identify the pathogen outside from a clinical setting, without the need of specialized personnel, in a cost-effective manner and by drastically reducing the time to respond. Such kind of point-of-care (POC) diagnostics are expected to allow rapid, robust and accurate infection diagnosis potentially improving patient care and disease surveillance, and reducing antimicrobial resistance, overall minimizing the effect of infectious

* Corresponding author. Department of Electronic Engineering, Universitat Rovira i Virgili, 43007, Tarragona, Spain.
** Corresponding author. Faculty of Pharmacy and Pharmaceutical Sciences, Monash University, Parkville, Melbourne, VIC, 3052, Australia.
E-mail addresses: nicolas.voelcker@monash.edu (N.H. Voelcker), bprieto@iciq.cat (B. Prieto-Simón).
[1] Author contributes equally to this work.

https://doi.org/10.1016/j.biosx.2024.100438
Received 2 August 2023; Received in revised form 17 November 2023; Accepted 3 January 2024
Available online 6 January 2024

disease outbreaks on public health (Hocking et al., 2021). Bacterial biomarkers such as the 16S rRNA genes are attractive bacterial biomarkers for the diagnosis of various infections due to their abundance in viable cells which help to skip culturing processes, save costs and time. Moreover, these genes are long RNA sequences featuring variable regions and others that are highly conserved across a wide range of bacterial species, making them useful biomarkers for identifying and classifying bacteria (Srinivasan et al., 2015). The accurate analysis of those sequences can lead to fragments that can be used to unambiguously identify a specific bacterial strain. These advantages endow specific 16S rRNA gene fragments with the potential to play a crucial role as biomarkers in the diagnosis of various bacterial infections, e.g., infections caused by *Escherichia coli* (*E. coli*) such as urinary tract infections (Nguyen et al., 2022; Quarata et al., 2023), autoimmune diseases (Lee et al., 2023), intra-abdominal infections, sepsis (Song et al., 2022), foodborne infections that cause gastroenteritis and hemolytic uremic syndrome (Lu et al., 2022), bacteremia (Bonten et al., 2021), etc. Due to their potential to overcome the limitations of current methods to detect bacteria, various POC tools have been reported targeting 16S rRNAs as biomarkers for bacterial infection diagnosis (De Felice et al., 2023; Liao et al. 2006, 2007; Liu et al., 2011; Miao and De Buck 2023; Pöhlmann et al., 2009; Wang et al., 2019). Specifically, genosensors have been widely explored because they meet the criteria for POC diagnostics, providing a versatile platform that can be modified to achieve the sensitivity and selectivity levels required. Nonetheless, the main limitations to use biosensors as POC tools involve difficulties in miniaturizing their transduction element, and to provide high sensitivity and specificity, the latter due to the challenges faced when analyzing clinical samples (Grieshaber et al., 2008; Varshney and Mallikarjunan 2009). To address these drawbacks, advances in the design of biosensors based on electrochemical transduction have effectively demonstrated their miniaturization, and the possibility to perform highly sensitive and specific measurements with small volumes of sample in a short time (Cheng et al., 2023; Kour et al., 2020; Liao et al. 2006, 2007; Wang et al., 2019).

Several electrochemical biosensors for the detection of 16S rRNA fragments have been reported in the literature. Most sensing strategies rely on signal amplification through the use of enzymes (Liao et al. 2006, 2007; Liu et al., 2011; Wang et al., 2019) or nanoparticles used as labels (Li et al., 2017; Lin et al., 2008; Seo et al., 2023; Sheng et al., 2016). However, the need to add multiple assay steps with lengthy incubation times and numerous washing steps to the analysis protocol increases analysis time, making it not compliant with POC device requirements (Chen et al., 2013; Li et al., 2017).

To suit POC requirements, the sensing strategy should ideally rely just on the affinity of the specific capture probe, omitting the need for labelling or signal amplification, which would require additional reagents or complex signal transduction methods. Sensing platforms built on porous materials have demonstrated their potential to facilitate the label- and amplification-free electrochemical detection of key biomarkers (Reta et al., 2018).

Porous silicon (pSi) in particular has attracted substantial attention for its use in sensing due to its high surface area, simple adjustability of pore diameter and depth, versatile surface chemistry and low-cost fabrication (Guo et al., 2022; Liu et al., 2018; Reta et al. 2016, 2018). Its large surface area has been shown to enhance the sensitivity of pSi-based biosensors compared to biosensors based on flat electrodes due to the increase in the density of available bioreceptors immobilized within the porous structure (Arshavsky Graham et al., 2020). To further enhance sensitivity, new sensing strategies have been explored that harness the possibility to use the pores as nanowells where to confine the analyte binding event (Liu et al., 2018; Reta et al. 2016, 2018). These strategies rely on quantifying the pore blockage caused by steric hindrance and electrostatic effects upon the analyte binding to the capture probe immobilized within the pores. By tuning pSi pore diameter, access of certain analytes within the porous structure can be favored, while that of large interfering species is prevented, enabling the pore blockage to be maximized and improving the overall selectivity of the biosensor.

Reta and co-workers reported for the first time a pSi-based electrochemical immunosensor for the detection of MS2 bacteriophage harnessing the pore blockage caused upon MS2 binding to the anti-MS2 antibodies immobilized within the porous structure as a sensing mechanism (Reta et al., 2016). The biosensor design consisted of a pSi membrane placed on a gold electrode acting as the electrochemical transducer. The developed pSi immunosensor not only provided high sensitivity, but also enabled the detection of the target microbial indicator in reservoir water samples without showing significant matrix effects. Nonetheless, such sensing configuration with a fragile pSi membrane resting on a gold electrode lacked robustness, making it very challenging to incorporate this platform into POC devices. To overcome this limitation, research efforts focused later on assessing configurations where the pSi film remained attached to the underlying Si substrate to improve the robustness of the sensing platform. To that purpose, pSi had to be modified to ensure its stability and ability to work both as biorecognition layer and electrochemical transducer (Guo et al., 2019).

Freshly etched pSi is surface-terminated by reactive hydride species, rapidly degrading when exposed to air or water (Dhanekar and Jain 2013; Salonen et al., 2000). Such lack of stability is not suitable for sensing purposes that involve measurements in aqueous environments. As a result, various methods have been reported to stabilize pSi, such as hydrosilylation and thermal oxidation. Of special interest for electrochemical sensing is the possibility to stabilize pSi by introducing Si–C bonds. Salonen et al. reported the stabilization of pSi via thermal treatment in the presence of acetylene gas which rendered the porous material with a chemically stable thin carbon layer all over the surface (Salonen et al., 2000). Our research group then proceeded to study in detail the electrochemical performance of pSi structures carbon-stabilized through the method reported by Salonen and colleagues: thermally hydrocarbonized pSi (THCpSi) and thermally carbonized pSi (TCpSi) (Guo et al., 2019; Tücking et al., 2018). Guo et al. worked with THCpSi and TCpSi, demonstrating both carbon-stabilized pSi structures exhibited excellent electron transfer kinetics, outperforming conventional carbon-based electrodes, such as glassy carbon and screen-printed carbon electrodes (Guo et al., 2019). THCpSi was then used as a proof of concept for the voltammetric detection of MS2 bacteriophage. The reported results underpinned the use of carbon-stabilized pSi as a highly efficient electrochemical transducer with the potential to significantly enhance the sensitivity of the biosensor. More recently, we demonstrated the feasibility to produce double-layer porous silicon structures to perform as electrochemical sensing platforms (Guo et al., 2022). Results showed the possibility to tune morphological features and surface functionalities of each layer, reporting a structure consisting of a top biorecognition layer and a bottom transducing layer, able to detect a short ssDNA used as model target analyte (Guo et al., 2022).

Here, we demonstrate for the first time a THCpSi-based biosensor, harnessing a pore blockage sensing strategy that enabled the ultrasensitive and label-free electrochemical detection of a specific 16S rRNA gene fragment, paving the way towards high-performing POC tools for the diagnosis of bacterial infections. THCpSi was used as a stable sensing platform which surface could be easily functionalized through alkene grafting, and simultaneously act as an electrochemical transducer (Del Tordello et al., 2012). The functionalization of THCpSi with undecylenic acid endowed its surface with the required functional groups for the immobilization of an amine-modified ssDNA capture probe complementary to a fragment of an *E. coli* 16S rRNA gene selected in this work as the key target analyte. The biosensor relied on the hybridization of the target RNA fragment to the ssDNA capture probe immobilized in the inner surface of the porous electrodes, causing partial pore blockage. Several optimization steps were followed to maximize the analytical performance of the developed biosensor, including tuning of pore diameter and film thickness, and ssDNA capture probe concentration. A

key optimization step involved the modification of the sensing platform as to ensure that hybridization was confined into the pores, to maximize sensitivity and minimize interferences when analyzing complex samples. Such modification consisted in introducing a thin Si_3N_4 layer as an external insulating coating of the pSi. Although the biosensor can be used to target a wide variety of 16S rRNA bacterial species, we here demonstrate the successful detection of a 28-base *E. coli*-specific 16S rRNA gene fragment, with a limit of detection (LOD) of 2.3 pM, and without showing significant matrix effects when analyzing 5% fetal bovine serum (FBS) samples spiked with the target RNA fragment.

2. Experimental section

***Reagents*:** Potassium ferrocyanide ($K_4[Fe(CN)_6]$), potassium ferricyanide ($K_3[Fe(CN)_6]$), undecylenic acid, N-hydroxysuccinimide (NHS), 1-ethyl-3-(3-dimethylaminopropyl) carbodiimide hydrochloride (EDC), phosphate buffered saline (PBS) tablets, sodium chloride (NaCl), Trizma hydrochloride, 2-(N-morpholino)-ethanesulfonic acid (MES), absolute ethanol, and ethanolamine were purchased from Sigma-Aldrich (Australia). Hydrofluoric acid (48%) of AR grade was purchased from Scharlau (Australia). The acetylene gas cylinder (1 m^3 industrial grade, dissolved) was purchased from BOC (Australia). All the oligonucleotides were purchased from Integrated DNA Technologies Pte Ltd (IDT Singapore), and their sequences are shown in Table S1 in Supplementary Information. The selected 16S rRNA gene fragment was previously reported as a good biomarker for *E. coli* detection (Purwidyantri et al., 2016).

***Fabrication of pSi*:** 6-inch p-type Si wafers with 0.00055–0.001 Ω cm resistivity, (100)-oriented, were purchased from Siltronix (France). A 6 inch p-type Si wafer with an exposed etching area of 132 cm^2 was anodically etched in 1:1 (v:v) 48% HF and absolute ethanol using a wet etching system (MPSB) to produce a pSi film. First, a current density of 60.6 mA/cm^2 was applied for 30 s to etch a sacrificial layer that was subsequently removed through exposure to 1 M sodium hydroxide (Guo et al., 2022). The sample was then rinsed with water, absolute ethanol and dried under a flow of N_2 gas. Next, various pSi samples were fabricated with fixed thickness and different pore diameters, by applying current densities and times of 53 mA/cm^2 for 60 s, 19 mA/cm^2 for 80 s and 12 mA/cm^2 for 300 s. Freshly etched pSi was also fabricated with fixed pore diameter and different thicknesses, by applying etching times of 60, 80 and 300 s and a constant current density of 19 mA/cm^2. All the samples were then rinsed with ethanol and were ready to proceed with thermal hydrocarbonization.

Stabilization of freshly etched pSi by thermal hydrocarbonization: Freshly etched pSi was stabilized through a thermal treatment that decomposes acetylene gas forming a protective carbon coating (Guo et al. 2019, 2022; Salonen et al., 2000). pSi was placed in a quartz tube where N_2 was flowed at 2 L/min for 45 min at room temperature to remove any traces of O_2. Next, a 1:1 N_2 and acetylene mixture was flowed into the quartz tube at room temperature for 15 min prior to and for 15 min after insertion into a pre-heated furnace at 525 °C. The final THCpSi sample was let to cool down to room temperature under N_2 flow.

***Scanning electron microscopy (SEM)*:** SEM was used to analyze pSi's pore diameter and film thickness. SEM images of pSi were obtained with a FEI NovaNano SEM 430 at an accelerating voltage of 5 kV.

***Fourier transform infrared spectroscopy (FTIR)*:** FTIR spectra of pSi after its stabilization, functionalization and modification were recorded with a Thermo Scientific Nicolet 6700 FTIR spectrometer with an average of 64 scans over the range of 750–4000 cm^{-1}.

***Electrochemical measurements*:** Electrochemical measurements were carried out with an Ivium-n-Stat potentiostat, with a qModule 30 mA/10 V (Netherlands). Measurements were performed using a three-electrode configuration system placed into a Teflon cell, connected to the analyzer, filled with a 2 mM $[Fe(CN)_6]^{3-}$ solution prepared in 10 mM PBS, pH 7.4. The electrodic system consists of a Pt wire as counter electrode, an Ag/AgCl as reference electrode and the modified THCpSi as the working electrode. Data analysis was performed using Ivium Software (Ivium Technologies, Eindhoven, The Netherlands). The electrochemical characterization was carried out via cyclic voltammetry (CV) and electrochemical impedance spectroscopy (EIS). CV was performed by scanning the potential from −0.3 V to 0.8 V at a scan rate of 0.1 V/s. EIS measurements were taken in a frequency range from 0.1 to 100 kHz, under open circuit potential condition, and at an AC amplitude of 5 mV. Electrochemical sensing was carried out via differential pulse voltammetry (DPV), by scanning the potential from −0.3 to 0.6 V at a scan rate of 0.1 V/s, pulse time of 200 ms, pulse amplitude of 50 mV and E step of 4 mV.

***Biosensor preparation*:** To allow covalently immobilizing the amino-modified ssDNA capture probe on THCpSi, first carboxylic groups were introduced on the THCpSi surface through thermal grafting. THCpSi was immersed into neat undecylenic acid at 150 °C for 10 h in an inert environment with continuous flow of N_2. After 10 h, the sample was cooled down to room temperature and rinsed with absolute ethanol (Guo et al., 2022).

To confine RNA hybridization to the inner part of the porous structure, the top surface of COOH-terminated THCpSi was subsequently modified with a thin layer of silicon nitride (Si_3N_4) through plasma enhanced vapor deposition (PECVD) (Oxford instruments system 100 PECVD). Si_3N_4 deposition was set at a rate of 22 nm/min and 250 °C, and applied for 7 s. The Si_3N_4-coated and uncoated COOH-terminated THCpSi platforms were activated by incubating the samples in a 1:1 mixture of 10 mg/mL EDC and 15 mg/mL NHS, prepared in 10 mM MES buffer at pH 5.5, during 30 min at room temperature. This step introduced succinimidyl ester groups on the surface of the THCpSi sample. Subsequently, a 10 μM solution of the amino-modified ssDNA capture probe prepared in 10 mM PBS at pH 7.4, was incubated on the activated surface for 16 h at 4 °C. The sample was then thoroughly rinsed with PBS prior to incubation with a 100 mM ethanolamine solution, prepared in 10 mM PBS, for 30 min to block the leftover active ester groups that did not covalently bind to the ssDNA capture probe. Control biosensors were prepared following the same protocol but using a random ssDNA sequence as the capture probe.

Si_3N_4 thickness deposition measurement: The thickness of the Si_3N_4 films deposited on a clean silicon wafer was measured using a spectroscopic ellipsometer (J.A. Woollam M-2000DI). The thickness of the films was calculated using a Cauchy optical model (Tompkins and Irene 2005).

***Water contact angle measurement*:** Water contact angle measurements were used to study the wettability of the pSi samples (Belorus et al., 2017). Contact angle of a water droplet on pSi after surface stabilization via carbonization was measured with a goniometer. The image was captured upon dropping 1 μL of MilliQ water with a 10 μL syringe onto the THCpSi surface. ImageJ software with contact angle analysis plugin was utilized to calculate the contact angle of the water droplet in contact with the THCpSi surfaces.

***Electrochemical detection of DNA*:** RNA is less stable than ssDNA making its synthesis and manipulation challenging, what increases its cost. RNA is more susceptible than ssDNA to environmental factors such as heat, UV light and RNases, making it vulnerable to degradation and decreasing its stability over time (Wang et al., 2014). As a result, initial sensing experiments devoted to performance optimization were performed with a 28-base ssDNA sequence equivalent to the 16S rRNA gene fragment selected as target analyte. Solutions of the target ssDNA prepared at various concentration from 0.1 pM to 1000 pM in 10 mM Tris buffer with 75 mM NaCl, pH 7.4 (TBS buffer), were incubated on the THCpSi biosensor for 15 min. After incubation, the target solution was removed and the biosensor surface was thoroughly rinsed with PBS. DPV measurements were performed, prior and after ssDNA incubation, in a 2 mM $[Fe(CN)_6]^{3-}$ solution prepared in 10 mM PBS, pH 7.4. All measurements were performed using three biosensors and three controls.

***Optimization of biosensor performance*:** To maximize the sensitivity of the biosensor developed, first the concentration of the ssDNA capture

probe used to modify the THCpSi substrates was optimized. Various biosensors were prepared by incubating different concentrations (5, 10, 25 μM) of the amino-modified ssDNA capture probe solution prepared in 10 mM PBS at pH 7.4, on the carbodiimide-activated surface of the Si_3N_4-modified COOH-terminated THCpSi for 16 h at 4 °C, as previously described. To further improve the sensitivity the effect of both pore diameter and film thickness was assessed. Biosensors with different pore diameters and a fixed thickness (pore diameter optimization), and biosensors with different thickness and a fixed pore diameter (thickness optimization) were prepared following the same protocol (refer to *Fabrication of pSi* section for further details).

Selectivity study: To assess the selectivity of the biosensor developed, its performance towards the detection of a 28-base ssDNA with sequence equivalent to that of the 16S rRNA gene fragment selected as target analyte, was compared to that against the detection of target oligonucleotides with 1-base and 2-base mismatches. The mismatched sequences were prepared at various concentration, from 0.1 pM to 1000 pM, in TBS buffer and incubated on the THCpSi biosensor for 15 min. Once the sensing platform was fully optimized with its selectivity assessed, its final performance was evaluated against the selected 16S rRNA target following the *Electrochemical detection of DNA* protocol (target ssDNA replaced with target 16S rRNA gene fragment).

Detection of 16S rRNA gene fragment in serum: Matrix effects when analyzing serum samples were tested by incubating target RNA solutions prepared at various concentration, from 0.1 pM to 1000 pM, in FBS diluted to 5% with TBS buffer on the optimized biosensor for 15 min.

3. Results and discussion

A label- and amplification-free 16S rRNA biosensor was built on a carbon stabilized pSi structure, specifically on THCpSi. THCpSi was selected as an ideal sensing platform due to, on the one hand, its excellent performance as electrochemical transducer (Guo et al., 2019; Tücking et al., 2018) and, on the other hand, its morphology conducive to designing biosensors based on a pore blockage sensing mechanism (Reta et al., 2018) (Fig. 1). To optimize the analytical performance of the biosensor, several parameters that can affect the sensitivity were studied. Apart from optimizing the ssDNA capture probe coverage of the biosensor surface, the performance of biosensors based on pore blockage can be optimized by tuning their morphology as to maximize the pore blockage caused upon analyte binding. To ensure the confinement of the hybridization event within the porous structure, a Si_3N_4-insulating layer was deposited on the outer surface of THCpSi. Next, pore diameter was adjusted to maximize pore blockage, followed by pSi film thickness optimization to maximize the transducing area.

Morphological characterization of pSi: The pore diameter and thickness of pSi fabricated via electrochemical anodization of 6-inch p-type crystalline silicon (100) were characterized with SEM. Pore diameter was controlled by tuning the current density applied where an increase in current density resulted in an increase in pore diameter (Sciacca et al., 2011). The etching rate or speed at which etching occurs increases upon increasing the current density (Cao et al., 2014). Therefore, keeping the thickness constant to investigate the pore diameter effect on the sensitivity of the biosensor, the etching time was varied to obtain the most suitable etching rate. Fig. 2A–C shows top-view SEM images of the pSi fabricated by applying (A) 53 mA/cm^2 for 60 s, (B) 19 mA/cm^2 for 80 s, and (C) 12 mA/cm^2 for 300 s, which resulted in average pore diameters of (A) 72 ± 15 nm, (B) 27 ± 9 nm, and (C) 12 ± 5 nm, respectively. The three pSi substrates showed a constant thickness of 1.6 μm.

pSi thickness was controlled by tuning the etching time applied where an increase in etching time resulted in a thicker pSi film (Behzad et al., 2012). The current density was kept constant at 19 mA/cm^2 while etching times were varied to study the effect of film thickness on the sensitivity of the biosensor. Fig. 2D–F shows SEM images of the cross-sectional view of the pSi fabricated by applying 19 mA/cm^2 for (D) 60 s, (E) 80 s, and (F) 300 s, which resulted in pSi films of a thickness of (D) 0.7 μm, (E) 1.6 μm, and (F) 3.4 μm, respectively. The three pSi substrates showed an average pore diameter of 27 nm.

Surface functionalization: The surface chemistry of both freshly etched pSi and THCpSi was first characterized with FTIR (Fig. S1). Next, the THCpSi substrate was functionalized to allow the covalent immobilization of the amino-modified ssDNA capture probe. As observed in Fig. 3, the FTIR spectrum of a THCpSi sample upon thermal grafting with undecylenic acid, shows three new bands at 1700 cm^{-1}, 2890 cm^{-1}, and 2940 cm^{-1}. These bands correspond to the C═O stretching vibrational mode of –COOH, stretching CH_2 and stretching vibrational mode of aliphatic C–H bonds, confirming the success of alkene grafting. Next, the COOH-terminated THCpSi surface was carbodiimide activated, forming a succinimidyl ester-terminated surface where a pronounced triplet band, with peaks at 1740 cm^{-1}, 1785 cm^{-1} and 1815 cm^{-1}, can be seen in the EDC/NHS spectrum of Fig. 3. This triplet band corresponds to the antisymmetric and symmetric C═O state of the carbonyl groups and the succinimidyl ester group (Sam et al., 2010). Bands at 1650 cm^{-1} and

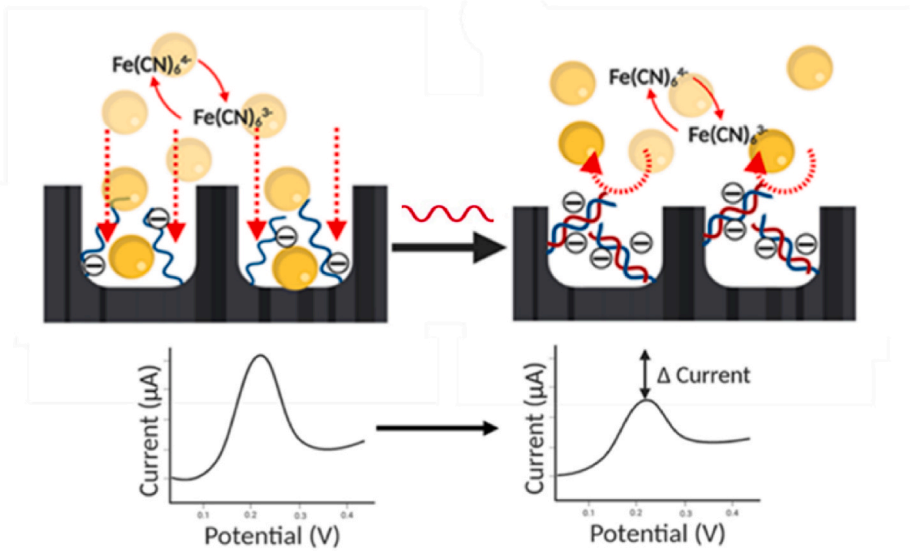

Fig. 1. Scheme of the sensing mechanism based on the pore blockage that occurs upon target hybridization to the ssDNA immobilized within the porous structure of THCpSi used for the label-free voltammetric detection of a 16S rRNA gene fragment, and the expected DPV response prior and after target hybridization.

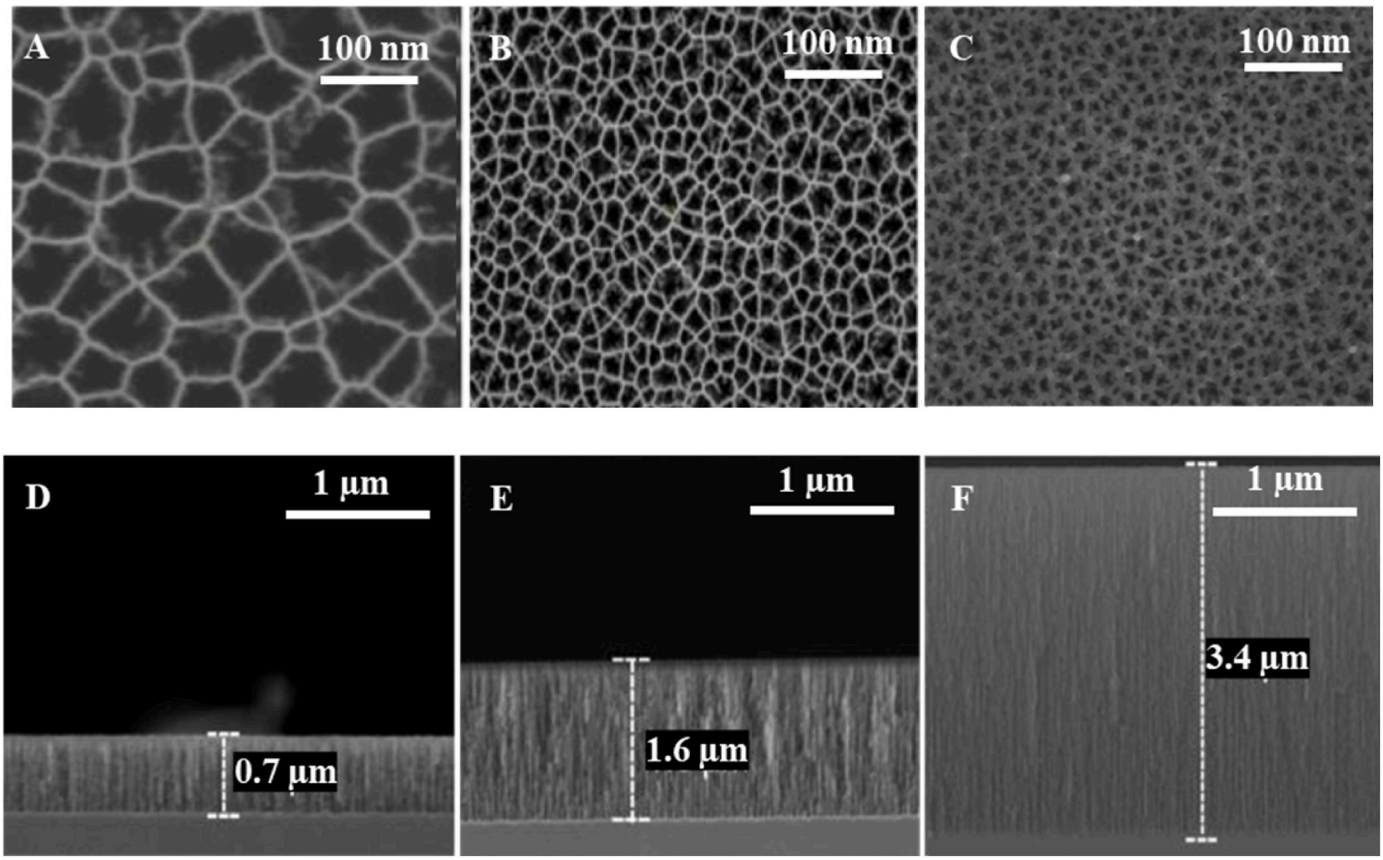

Fig. 2. (A–C) Top-view SEM images of pSi prepared through electrochemical anodization in 1:1 HF:ethanol by applying a current density of (A) 53 mA/cm^2 for 60 s, (B) 19 mA/cm^2 for 80 s, and (C) 12 mA/cm^2 for 300 s, which resulted in average pore diameters of (A) 72 ± 15 nm, (B) 27 ± 9 nm, and (C) 12 ± 5 nm, respectively. (D–F) Cross-sectional view SEM images of pSi prepared by applying 19 mA/cm^2 for (D) 60 s, (E) 80 s, and (F) 300 s, which resulted in pSi films of a thickness of (D) 0.7 μm, (E) 1.6 μm, and (F) 3.4 μm, respectively.

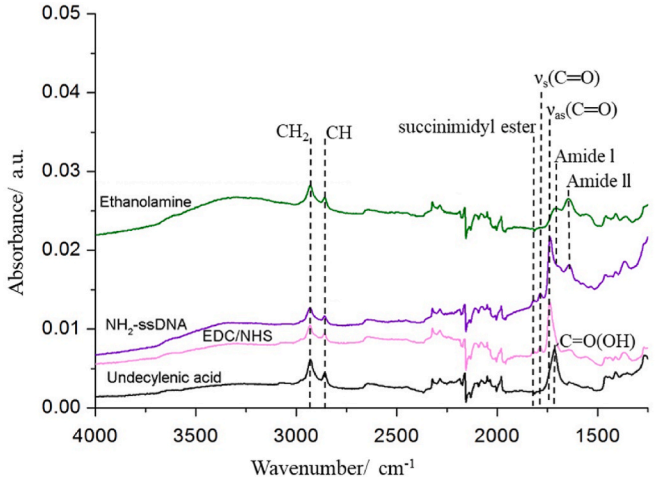

Fig. 3. FTIR spectra of THCpSi after undecylenic acid thermal grafting (black), carbodiimide activation with EDC/NHS (pink), amino-modified ssDNA capture probe immobilization (purple) and deactivation of remaining succinimidyl ester groups with ethanolamine (green). (For interpretation of the references to colour in this figure legend, the reader is referred to the Web version of this article.)

1550 cm^{-1} in the spectrum of the sample after incubation with NH_2-ssDNA represent the peptide C═O stretch (amide I) and peptide N–H bend (amide II). These peaks demonstrated the successful immobilization of the ssDNA capture probe to the surface. After quenching with ethanolamine, the pronounced triplet band is no longer visible in the corresponding spectrum in Fig. 3. This indicates that the unreacted NHS-ester groups were successfully quenched with ethanolamine. The immobilization of the ssDNA capture probe on THCpSi was also supported by the electrochemical characterization results shown in Fig. S3.

Optimization of biosensor performance for DNA detection: To facilitate the process required to thoroughly optimize the developed sensing platform, all experiments were initially performed using a ssDNA sequence equivalent to the target 16S rRNA gene fragment. Once the optimization process was completed, the electrochemical response of the final biosensor was evaluated against the detection of the target 16S rRNA gene fragment. Fig. 1 depicts the sensing mechanism based on the pore blockage caused upon target hybridization harnessed in this work. Sensing is based on hybridization to the ssDNA capture probe immobilized within the inner part of the porous structure causing a partial pore blockage. DPV measurements were recorded before and after analyte incubation, where a reduction in the I_{ox} of the redox species $[Fe(CN)_6]^{3-/4-}$ added to the measuring solution was observed, which was attributed to their hindered diffusion towards the transducer surface when pores were partially blocked.

The change in current intensity (ΔI) before and after analyte incubation was normalized by applying the following equation:

$$\Delta I = (I_0 - I_i)/I_0$$

Where I_0 is the current intensity value measured after incubation in TBS buffer, and I_i is the current intensity value measured after 15-min incubation in a target DNA/RNA solution prepared in the same TBS buffer. Dose-response curves were plotted as ΔI values vs Log [target analyte] to determine the sensitivity of the biosensor. Sensitivity values were used

to compare the performance of the various biosensors developed during the optimization process. The response of the biosensors was always compared to that shown by control biosensors prepared with a ssDNA capture probe non-complementary to the target analyte to confirm its reliability and accuracy.

Si_3N_4-coated vs uncoated THCpSi: The effect of depositing Si_3N_4 on the outer surface of the biosensor was investigated by comparing the performance of the biosensor with and without Si_3N_4 (Fig. S6). The presence of a thin Si_3N_4 layer on the outer surface of the THCpSi substrate is expected to limit the immobilized capture probe to binding to the inner porous structure, and thus confines the hybridization event within the pores, and maximizing pore blockage. Indeed, this effect is confirmed by the improved sensitivity of the Si_3N_4-coated biosensor compared to that of the uncoated biosensor as depicted in Fig. S6. In that case, THCpSi featuring a pore diameter of 27 ± 9 nm and a film thickness of 1.6 μm was modified with a thin Si_3N_4 coating prior to carbodiimide activation and modification by incubating a 10 μM DNA capture probe solution. Sensing performance of Si_3N_4-coated and uncoated biosensors was compared. As shown in Fig. S6, the presence of a Si_3N_4 layer on the top surface of the biosensor ($y = 0.1210*\log$ [DNA target] + 0.3890, $R^2 = 0.9900$) improved the sensitivity by more than 2-fold that shown by an equivalent uncoated biosensor ($y_2 = 0.0565*\log$ [DNA target] + 0.1493, $R^2 = 0.9604$). As Si_3N_4 is an electrically insulating material with high hydrophilicity, interfacial reactions/non-specific binding can be reduced (Lei et al., 1997). As observed in Fig. S4 from supporting information, THCpSi with a thin Si_3N_4 layer deposited at the outer surface of the pores is more hydrophilic than uncoated THCpSi, underpinning the viability of Si_3N_4 to minimize the non-specific binding of species that might interfere in the sensing response. The thickness of the Si_3N_4 layer was measured via ellipsometric measurements (Fig. S5). This is the first time that analyte binding confinement within pores is shown to enhance the sensitivity of porous biosensors relying on a pore blockage sensing mechanism for the electrochemical quantification of analytes. As a result, Si_3N_4-coated THCpSi substrates were used in the following optimization studies to maximize pore blockage and thus achieve the highest sensitivity.

Optimization of THCpSi pore diameter: Pore diameter must be large enough to enable the access of the capture probe to be covalently immobilized to the inner part of the pores during biosensor preparation, and the penetration of the analyte into the pores to hybridize the immobilized probe during sensing. Once analyte access to the pores is guaranteed, the pore diameter of THCpSi can be finely tailored to maximize the pore blockage caused by target analyte hybridization, and thus improve the sensitivity of the sensor. In addition, pore diameter can also help minimize interferences, by adjusting its size to be small enough to prevent the access of large interfering species present in the sample through size-exclusion effects (RoyChaudhuri 2015).

The effect of maximizing pore blockage and the filtering capability can be combined to enhance biosensor performance by increasing sensitivity and reducing matrix effects when working with real samples. To select the optimum pore diameter for a 28-base oligonucleotide target which is roughly 9 nm (de la Escosura-Muñiz and Merkoçi 2011), freshly etched pSi samples with three pore diameters, 72 ± 15 nm, 27 ± 9 nm and 12 ± 5 nm, and with constant thickness of 1.6 μm (Fig. 2A–C), were prepared. pSi samples were thermally hydrocarbonized, and then modified by the deposition of a Si_3N_4 layer before immobilizing the ssDNA capture probe using a 10 μM solution, which was optimized previously (Fig. S7). The pSi pore diameter remained unaltered after thermal hydrocarbonization (Guo et al., 2019), but it shrunk to 69 ± 14 nm, 25 ± 8 nm, and 10 ± 5 nm, respectively, after Si_3N_4 deposition (Fig. S2). Fig. 4 shows the effect of pore diameter on the performance of the biosensor. Comparing the three different pore diameters tested, biosensors prepared from freshly etched pSi featuring a pore diameter of 25 nm showed the highest sensitivity, as analyzed from the slope of the dose-response curves in Fig. 4 ($y = 0.1233*$Log [target DNA] + 0.1939). Biosensors featuring a pore diameter of 25 nm showed sensitivity values

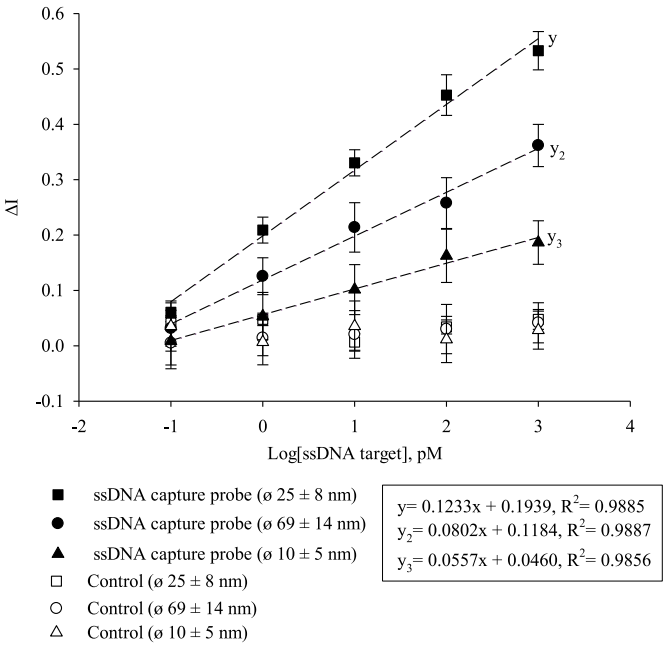

Fig. 4. Dose-response curves obtained using Si_3N_4-coated THCpSi biosensors and control sensors prepared with structures featuring an average pore diameter of 69 ± 14 nm, 25 ± 8 nm or 10 ± 5 nm, and a film thickness of 1.6 μm. 10 μM ssDNA capture probe was used. Biosensors and controls were tested in triplicates, n = 3. Data are shown as mean of the normalized current intensity ± the associated standard deviation.

54 % and 121 % higher than those achieved by biosensors with average pore diameters of 69 nm and 10 nm, respectively. The optimum pore diameter allowed access of the analyte and hybridization to the immobilized capture probe. It is hypothesized that pore blockage was mainly driven by the electrostatic repulsion between the hybridized oligonucleotide and the $[Fe(CN)_6]^{3-/4-}$ redox pair added to the measuring solution, the latter being hindered from diffusing to the transducer surface.

When the average pore diameter increased to 69 nm, there was ample space for the target DNA molecules to diffuse and hybridize to the capture probe immobilized in the pores, but the electrostatic and steric effects to block the pores were not as prominent. As such, the redox species could still diffuse towards the transducer surface to undergo oxidation. In contrast, when pore diameter decreased to 10 nm, the diffusion of the target DNA molecules within the pores was restricted, hampering their hybridization to the immobilized ssDNA capture probe and thus causing less effect on pore blockage.

Optimization of THCpSi film thickness: The tunability of THCpSi film thickness allows the surface area of the biosensor to be adjusted, and this is expected to impact significantly on the sensing performance. On the one hand, the larger surface area of thicker films allows more bioreceptors to be immobilized with the right distribution (RoyChaudhuri 2015). On the other hand, the whole biosensor, excluding the Si_3N_4-coated region, performs as electrochemical transducer, and thus increasing film thickness results in a larger active transducer area. Combining both effects can increase the measured signal. Nonetheless, for very thick films diffusion of the target analyte into the deeper regions may be an issue. As such, it is important to find the optimum THCpSi film thickness to develop the biosensor with the highest sensitivity. To select the optimum film thickness, pSi samples with three film thicknesses, 0.7 μm, 1.6 μm and 3.4 μm, and with a constant pore diameter of 27 ± 9 nm (Fig. 2D–F), were prepared. All pSi samples were thermally hydrocarbonized, followed by deposition of Si_3N_4 before immobilizing the DNA capture probe using a 10 μM solution, which was optimized previously (Fig. S7). The dose-response curves displayed in Fig. 5 show the effect of film thickness on the performance of the biosensor (note

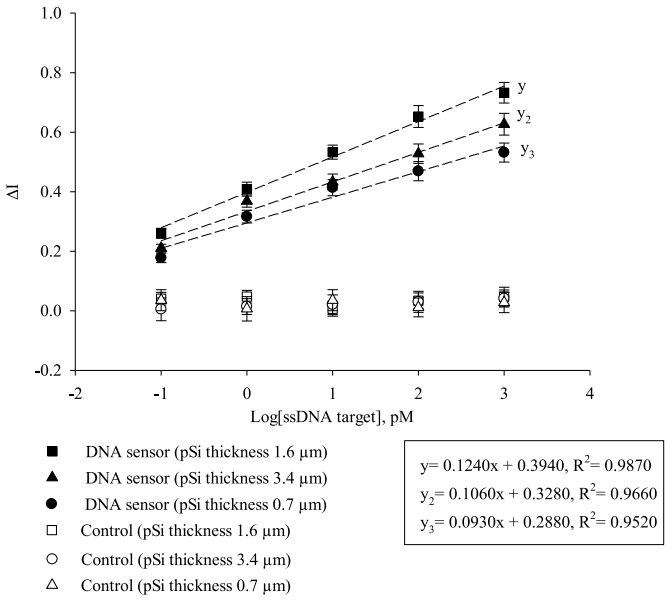

Fig. 5. Dose-response curves obtained using Si_3N_4-coated THCpSi biosensors and control sensors prepared with structures featuring a film thickness of 0.7 µm, 1.6 µm or 3.4 µm, and an average pore diameter of 25 ± 8 nm. 10 µM ssDNA capture probe was used. Biosensors and controls were tested in triplicates, n = 3. Data are shown as mean of the normalized current intensity ± the associated standard deviation.

that curves show an upward translation compared to those in Fig. 4, accounting for the lower background current values of this specific set of biosensors). Biosensors featuring a THCpSi film thickness of 1.6 µm ($y = 0.1204*\log$ [DNA target] + 0.3940, $R^2 = 0.9870$) showed the highest sensitivity as observed from the slope of their dose-response curve. The sensitivity achieved with THCpSi biosensors featuring a film thickness of 1.6 µm was 14% and 33% higher than those shown by biosensors with 3.4 µm ($y_2 = 0.1060*\log$ [DNA target] + 0.3280, $R^2 = 0.9660$) and 0.7 µm ($y_3 = 0.0930*\log$ [DNA target] + 0.2880, $R^2 = 0.9520$) depth, respectively. On the one hand, thin THCpSi films, such as those with 0.7 µm thickness had limited surface area. This means that less immobilized bioreceptors were available for hybridization. Moreover, since THCpSi was acting as electrochemical transducer, reducing film thickness meant decreasing the active surface area. The combination of these two effects translated into low signal responses. On the other hand, thick THCpSi films, such as those with 3.4 µm, had a large surface and thus a large number of bioreceptors were available for hybridization. However, by increasing film thickness, the free diffusion of capture probe first, and later of the target analyte, could be hindered along the long and narrow pores. The decrease in sensitivity observed for the 3.4 µm-thick THCpSi biosensor compared to that of biosensors prepared from 1.6 µm-thick THCpSi, might be attributed to those diffusion limitations. Therefore, biosensors featuring a THCpSi film thickness of 1.6 µm were chosen as the optimum, producing the most sensitive response for DNA detection as shown in Fig. 5.

Selectivity study of the optimum biosensor: To accurately diagnose a bacterial infection selectivity is key. Any false positive results shown by the biosensor in response to oligonucleotide sequences that are not fully complementary to the immobilized capture probe, must be avoided. As such, it is extremely important to develop highly selective biosensors. Once the THCpSi-based biosensor was optimized to show the highest sensitivity, its selectivity was investigated by comparing the response towards the target analyte (complementary to the capture probe) to that obtained upon incubation of solutions of target ssDNA sequences with 1- and 2-base mismatches. The sensitivity of the biosensor for the detection of the fully complementary target analyte was 7 and 7.4 times higher than that shown when the biosensor was exposed to DNA sequences with 1- and 2-base mismatches (Fig. S8). These results confirm the excellent selectivity of the biosensor for the detection of a ssDNA with a sequence equivalent to the target 16S rRNA fragment.

Biosensor performance against RNA detection: Once a sensor targeting a ssDNA sequence equivalent to the selected *E. coli* 16S rRNA fragment was developed, showing high sensitivity and accuracy, the next step was to demonstrate its potential to detect RNA. The selected fragment from the *E. coli* 16S rRNA gene was used as the target RNA analyte. It is important to note that the platform can be easily tailored to other RNA fragments from 16S rRNA genes identified as bacterial biomarkers just by changing the sequence of the immobilized ssDNA capture probe. To evaluate the biosensor's performance towards RNA detection, dose-response curves were obtained by incubating the biosensor with increasing concentrations of the target RNA. As shown in Fig. 6, the dose-response curve of the developed biosensor when testing the target RNA, provided a linear response ($y = 0.0732*\text{Log}$ [16S rRNA] + 0.1412) over a dynamic range from 0.1 pM to 1000 pM. The biosensor showed a theoretical LOD of 2.3 pM which was calculated as the concentration providing a signal equal to three times the standard deviation associated to the measured signal in the absence of target analyte (Shrivastava and Gupta 2011).

It is important to highlight that the sensitivity of the biosensor towards the detection of the target RNA was 40% lower than that obtained against the target ssDNA. This might be attributed to several factors related to the experimental conditions in which the experiments were performed, being of special concern the poor stability of RNA. RNA is more chemically and thermally labile than DNA, and thus more susceptible to be degraded. Moreover, RNA can be degraded via RNases which are ubiquitous in the environment (Wang et al., 2014). To ensure the developed biosensors could be used as a point-of-testing tool, although most plasticware used was sterilized, all solutions were prepared with MilliQ water instead of diethylpyrocarbonate (DEPC)-treated water, and chemicals were not of RNase-free quality. Those working conditions do not guarantee an RNase-free environment, what could have led to a reduced sensitivity when analyzing RNA samples.

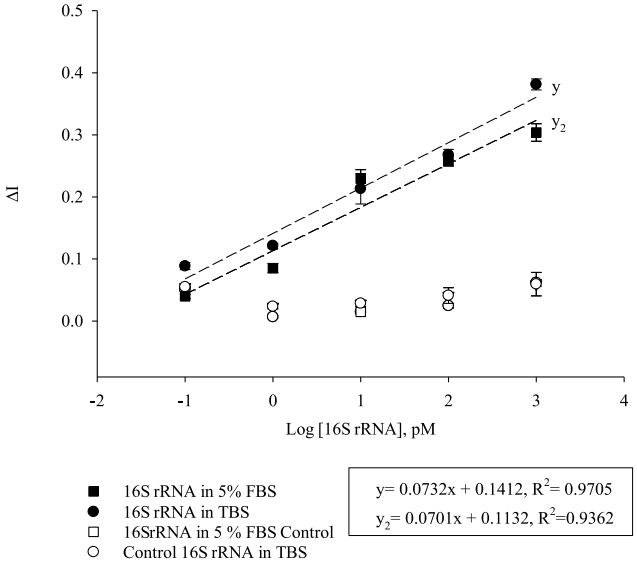

Fig. 6. Detection of the target 16S rRNA fragment prepared in TBS buffer, and in a 5% FBS solution, using the optimized Si_3N_4-coated THCpSi-based biosensor and corresponding control biosensor, both featuring pore diameter of 25 ± 8 nm and thickness of 1.6 µm. Experiments were performed in triplicate, n = 3. Data are shown as mean of the normalized current intensity ± the associated standard deviation.

Nonetheless, the analytical performance and robustness of our biosensor are comparable, if not better, with improved LOD and shorter detection time (15 min), to some previous publications reporting the electrochemical detection of 16S rRNA gene fragments (between 1 and 2 h) (Henihan et al., 2016; Purwidyantri et al. 2016, 2017).

Study of matrix effects when analyzing biological samples with the optimized biosensor: It is of utmost importance to evaluate potential matrix effects on the biosensor response when challenged with complex biological samples such as serum (Masson 2020). This is to evaluate the consequence of having interfering species in the biological sample to be analyzed as they can have a detrimental effect on the performance of the biosensor. Bacteria can be found directly in the blood of an infected patient where pre-treatment methods are usually required to detect its RNA which can be used to detect different strains of bacteria species (Del Tordello et al., 2012; Rogacs et al., 2012). Therefore, it is vital to investigate if the optimized biosensor might suffer matrix effects when attempting the detection of 16S rRNA in serum. To evaluate matrix effects, a 5% FBS solution prepared in TBS buffer was spiked with various concentrations of the target 16S rRNA fragment. The dose-response curves for the detection of the selected 16S rRNA fragment both in TBS buffer and in 5% FBS are shown in Fig. 6. It is observed that the signal obtained in serum slightly deviates from linearity as the concentration of 16S rRNA increases. This effect might be attributed to the longer exposure of the sensor surface to serum, as measurements in solutions with increasing concentrations of 16S rRNA were performed consecutively following multiple incubation steps. Nonetheless, even taking into account that slight deviation from linearity, there is an excellent agreement between the sensitivity of the dose-response curves in TBS buffer and 5% serum, with only a 4% decrease for the latter ($P = 0.648$, no significant difference). Therefore, matrix effects when working with 5% FBS can be neglected, underpinning the potential and robustness of this biosensor for detecting 16S rRNA genes from a biological sample. These results provide a strong foundation for the future application of the biosensor to detect key 16S rRNA gene fragments in a clinical sample which is expected to involve thermal lysis of bacteria, and removal of supernatant through centrifugation prior to RNA cleavage to obtain the crude intercellular matrix which will be used for 16S rRNA detection (Imani et al., 2023). The theoretical LOD achieved with the optimized biosensor is lower than the LODs reported for other electrochemical biosensors applied for the detection of isolated 16S rRNA from clinical samples (Khalifa et al., 2019; Mohan et al., 2011), confirming its potential to accurately quantify 16S rRNA fragments isolated from clinical samples as reported above. For example, an electrochemical sensor modified with polyaniline and gold nanoparticles, managed to enhance electrical conductivity of the biosensor and detected a key 16S rRNA from patient samples with bacterial cornea ulcer achieving a LOD of 500 nM (Khalifa et al., 2019). A target 16S rRNA was also successfully detected from urine samples of patients with urinary tract infection on an electrochemical biosensor array with a LOD between 2 and 20 pM for urinary tract infection diagnosis (Mohan et al., 2011).

4. Conclusions

In this study, we report a carbon-stabilized pSi biosensor, based on a pore-blockage sensing mechanism, able to sensitively detect through electrochemical means a specific 16S rRNA fragment. The fully optimized biosensor achieved a LOD that exceeds the values shown by other electrochemical biosensors for 16S rRNA detection (Khalifa et al., 2019; Mohan et al., 2011). Moreover, the reported biosensor beats many other electrochemical biosensors based on signal amplification in terms of simplicity and detection time (Liao et al. 2006, 2007; Liu et al., 2011; Wang et al., 2019). When compared to similar DNA sensing strategies based on pore blockage as sensing mechanism, the literature mostly reports porous alumina-based sensing platforms (Chaturvedi et al., 2016; Koh et al., 2007; Nguyen et al., 2009) with scarcity reported on pSi-based platforms where all are membrane-based and required an additional conductive support (e.g., gold) used as electrochemical transducer (Reta et al., 2016). These membrane-based sensors lack robustness, hindering their translation into cost-effective and friendly-user devices. In this paper, we demonstrate the sensitivity of robust and easy-to-fabricate THCpSi can be improved by depositing a Si_3N_4 insulating coating on the outer surface of the THCpSi structure, which restricts hybridization to occur within the pores and, thus, only those hybridization events contribute to pore blockage. Despite the sensitivity not being comparable to established techniques such as PCR where DNA can be detected in the fM range (Zou et al., 2018), the optimized biosensor allowed rapid analysis of 16S rRNA fragments in 15 min compared to the lengthy complicated process of PCR. The low LOD, good selectivity, short response time, and the possibility to work in diluted serum samples without significant matrix effects show this sensing platform as a promising method to identify specific species of bacteria in real samples upon their thermal lysis.

CRediT authorship contribution statement

Grace Pei Chin: Formal analysis, Investigation, Writing – original draft. **Keying Guo:** Formal analysis, Investigation, Supervision, Writing – review & editing. **Roshan Vasani:** Supervision. **Nicolas H. Voelcker:** Conceptualization, Funding acquisition, Supervision, Writing – review & editing. **Beatriz Prieto-Simón:** Conceptualization, Funding acquisition, Project administration, Supervision, Writing – review & editing.

Declaration of competing interest

The authors declare that they have no known competing financial interests or personal relationships that could have appeared to influence the work reported in this paper.

Data availability

Data will be made available on request.

Acknowledgments

G.P.C. acknowledges funding by a Monash University Graduate Scholarship 01138234. B.P.S. acknowledges financial support from grant PID 2021-124867OB-I00 funded by MCIN/AEI/10.13039/501100011033 and, by "ERDF A way of making Europe", and from the Generalitat de Catalunya (2021 SGR 00223). The authors also acknowledge funding from the Probing Biosystems Future Science Platform of the CSIRO. This work was performed in part at the Melbourne Centre for Nanofabrication (MCN) in the Victorian Node of the Australian National Fabrication Facility (ANFF).

Appendix A. Supplementary data

Supplementary data to this article can be found online at https://doi.org/10.1016/j.biosx.2024.100438.

References

Arshavsky Graham, S., Boyko, E., Salama, R., Segal, E., 2020. Mass transfer limitations of porous silicon-based biosensors for protein detection. ACS Sens. 5 (10), 3058–3069.

Behzad, K., Mat Yunus, W.M., Talib, Z.A., Zakaria, A., Bahrami, A., Shahriari, E., 2012. Effect of etching time on optical and thermal properties of p-type porous silicon prepared by electrical anodisation method. Adv. Opt. Technol. 2012 https://doi.org/10.1155/2012/581743, 581743.

Belorus, A., Bukina, Y., Pastukhov, A., Stebko, D., Spivak, Y.M., Moshnikov, V., 2017. Investigation of porous silicon obtained under different conditions by the contact angle method. Journal of Physics: Conference Series. IOP Publishing, 012051.

Bloom, D.E., Cadarette, D., 2019. Infectious disease threats in the twenty-first century: strengthening the global response. Front. Immunol. 10, 549.

Bonten, M., Johnson, J.R., van den Biggelaar, A.H., Georgalis, L., Geurtsen, J., de Palacios, P.I., Gravenstein, S., Verstraeten, T., Hermans, P., Poolman, J.T., 2021.

Epidemiology of Escherichia coli bacteremia: a systematic literature review. Clin. Infect. Dis. 72 (7), 1211–1219.
Cao, A.T., Luong, Q.N.T., Dao, C.T., 2014. Influence of the anodic etching current density on the morphology of the porous SiC layer. AIP Adv. 4 (3), 037105.
Chaturvedi, P., Rodriguez, S.D., Vlassiouk, I., Hansen, I.A., Smirnov, S.N., 2016. Simple and versatile detection of viruses using anodized alumina membranes. ACS Sens. 1 (5), 488–492.
Chen, Y., Wang, Q., Xu, J., Xiang, Y., Yuan, R., Chai, Y., 2013. A new hybrid signal amplification strategy for ultrasensitive electrochemical detection of DNA based on enzyme-assisted target recycling and DNA supersandwich assemblies. Chem. Commun. 49 (20), 2052–2054.
Cheng, L., Yang, F., Zhao, Y., Liu, Z., Yao, X., Zhang, J., 2023. Tetrahedron supported CRISPR/Cas13a cleavage for electrochemical detection of circular RNA in bladder cancer. Biosens. Bioelectron. 222, 114982.
De Felice, M., De Falco, M., Serra, A., Frisulli, V., Antonacci, A., Isticato, R., de Stefano, L., Scognamiglio, V., 2023. Fighting nosocomial antibiotic-resistant infections through rapid and sensitive isothermal amplification-powered point-of-care (POC) diagnostics. TrAC, Trends Anal. Chem., 117135
de la Escosura-Muñiz, A., Merkoçi, A., 2011. A nanochannel/nanoparticle-based filtering and sensing platform for direct detection of a cancer biomarker in blood. Small 7 (5), 675–682.
Del Tordello, E., Bottini, S., Muzzi, A., Serruto, D., 2012. Analysis of the regulated transcriptome of Neisseria meningitidis in human blood using a tiling array. J. Bacteriol. 194 (22), 6217–6232.
Dhanekar, S., Jain, S., 2013. Porous silicon biosensor: current status. Biosens. Bioelectron. 41, 54–64.
Grieshaber, D., MacKenzie, R., Vörös, J., Reimhult, E., 2008. Electrochemical biosensors-sensor principles and architectures. Sensors 8 (3), 1400–1458.
Guo, K., Alba, M., Chin, G.P., Tong, Z., Guan, B., Sailor, M.J., Voelcker, N.H., Prieto-Simón, B., 2022. Designing electrochemical biosensing platforms using layered carbon-stabilized porous silicon nanostructures. ACS Appl. Mater. Interfaces 14 (13), 15565–15575.
Guo, K., Sharma, A., Toh, R.J., Alvárez de Eulate, E., Gengenbach, T.R., Cetó, X., Voelcker, N.H., Prieto-Simón, B., 2019. Porous silicon nanostructures as effective faradaic electrochemical sensing platforms. Adv. Funct. Mater. 29 (24), 1809206.
Henihan, G., Schulze, H., Corrigan, D.K., Giraud, G., Terry, J.G., Hardie, A., Campbell, C. J., Walton, A.J., Crain, J., Pethig, R., 2016. Label-and amplification-free electrochemical detection of bacterial ribosomal RNA. Biosens. Bioelectron. 81, 487–494.
Hocking, L., George, J., Broberg, E.K., Struelens, M.J., Leitmeyer, K.C., Deshpande, A., Parkinson, S., Francombe, J., Morley, K.I., de Carvalho Gomes, H., 2021. Point of care testing for infectious disease in Europe: a scoping review and survey study. Front. Public Health 9, 722943.
Imani, S.M., Osman, E., Bakhshandeh, F., Qian, S., Sakib, S., MacDonald, M., Gaskin, M., Zhitomirsky, I., Yamamura, D., Li, Y., 2023. Liquid NanoBiosensors enable one-pot electrochemical detection of bacteria in complex matrices. Adv. Sci., 2207223
Khalifa, M.M., Elkhawaga, A.A., Hassan, M.A., Zahran, A.M., Fathalla, A.M., El-Said, W. A., El-Badawy, O., 2019. Highly specific Electrochemical Sensing of Pseudomonas aeruginosa in patients suffering from corneal ulcers: a comparative study. Sci. Rep. 9 (1), 18320.
Koh, G., Agarwal, S., Cheow, P.-S., Toh, C.-S., 2007. Development of a membrane-based electrochemical immunosensor. Electrochim. Acta 53 (2), 803–810.
Kour, R., Arya, S., Young, S.-J., Gupta, V., Bandhoria, P., Khosla, A., 2020. Recent advances in carbon nanomaterials as electrochemical biosensors. J. Electrochem. Soc. 167 (3), 037555.
Lee, H.J., Lee, S.W., Cha, H.R., Ha, E.K., Kim, J.H., Shin, S.Y., Lee, K.C., Leung, P.S., Han, M.Y., Choi, J.J., 2023. Acquired susceptibility to autoimmune diseases in pediatric patients with Escherichia coli infection: a population-matched retrospective cohort study. J. Autoimmun., 102997
Lei, J.-F., Martin, L.C., Will, H.A., 1997. Advances in Thin Film Sensor Technologies for Engine Applications. American Society of Mechanical Engineers.
Li, Y., Xiong, Y., Fang, L., Jiang, L., Huang, H., Deng, J., Liang, W., Zheng, J., 2017. An electrochemical strategy using multifunctional nanoconjugates for efficient simultaneous detection of Escherichia coli O157: H7 and Vibrio cholerae O1. Theranostics 7 (4), 935.
Liao, J.C., Mastali, M., Gau, V., Suchard, M.A., Møller, A.K., Bruckner, D.A., Babbitt, J.T., Li, Y., Gornbein, J., Landaw, E.M., 2006. Use of electrochemical DNA biosensors for rapid molecular identification of uropathogens in clinical urine specimens. J. Clin. Microbiol. 44 (2), 561–570.
Liao, J.C., Mastali, M., Li, Y., Gau, V., Suchard, M.A., Babbitt, J., Gornbein, J., Landaw, E. M., McCabe, E.R., Churchill, B.M., 2007. Development of an advanced electrochemical DNA biosensor for bacterial pathogen detection. J. Mol. Diagn. 9 (2), 158–168.
Lin, Y.-H., Chen, S.-H., Chuang, Y.-C., Lu, Y.-C., Shen, T.Y., Chang, C.A., Lin, C.-S., 2008. Disposable amperometric immunosensing strips fabricated by Au nanoparticles-modified screen-printed carbon electrodes for the detection of foodborne pathogen Escherichia coli O157: H7. Biosens. Bioelectron. 23 (12), 1832–1837.
Liu, C., Zeng, G.-M., Tang, L., Zhang, Y., Li, Y.-P., Liu, Y.-Y., Li, Z., Wu, M.-S., Luo, J., 2011. Electrochemical detection of Pseudomonas aeruginosa 16S rRNA using a biosensor based on immobilized stem–loop structured probe. Enzym. Microb. Technol. 49 (3), 266–271.
Liu, Y., Liu, Y., Qiao, L., Liu, Y., Liu, B., 2018. Advances in signal amplification strategies for electrochemical biosensing. Curr. Opin. Electrochem. 12, 5–12.
Lu, Z., Liu, Z., Li, X., Qin, X., Hong, H., Zhou, Z., Pieters, R.J., Shi, J., Wu, Z., 2022. Nanobody-based bispecific neutralizer for shiga toxin-producing E. coli. ACS Infect. Dis. 8 (2), 321–329.
Masson, J.-F., 2020. Consideration of Sample Matrix Effects and "Biological" Noise in Optimizing the Limit of Detection of Biosensors. ACS Publications, pp. 3290–3292.
Miao, Z., De Buck, J., 2023. Biosensor for PCR amplicons by combining split trehalase and DNA-binding proteins: a proof of concept study. J. Microbiol. Methods, 106780.
Mohan, R., Mach, K.E., Bercovici, M., Pan, Y., Dhulipala, L., Wong, P.K., Liao, J.C., 2011. Clinical validation of integrated nucleic acid and protein detection on an electrochemical biosensor array for urinary tract infection diagnosis. PLoS One 6 (10), e26846.
Nguyen, B.T., Koh, G., Lim, H.S., Chua, A.J., Ng, M.M., Toh, C.-S., 2009. Membrane-based electrochemical nanobiosensor for the detection of virus. Anal. Chem. 81 (17), 7226–7234.
Nguyen, S.N., Thi Le, H.T., Tran, T.D., Vu, L.T., Ho, T.H., 2022. Clinical epidemiology characteristics and antibiotic resistance associated with urinary tract infections caused by E. coli. International journal of nephrology, 2022.
Pöhlmann, C., Wang, Y., Humenik, M., Heidenreich, B., Gareis, M., Sprinzl, M., 2009. Rapid, specific and sensitive electrochemical detection of foodborne bacteria. Biosens. Bioelectron. 24 (9), 2766–2771.
Purwidyantri, A., Chen, C.-H., Chen, L.-Y., Chen, C.-C., Luo, J.-D., Chiou, C.-C., Tian, Y.-C., Lin, C.-Y., Yang, C.-M., Lai, H.-C., 2017. Speckled zno nanograss electrochemical sensor for staphylococcus epidermidis detection. J. Electrochem. Soc. 164 (6), B205.
Purwidyantri, A., Chen, C.-H., Hwang, B.-J., Luo, J.-D., Chiou, C.-C., Tian, Y.-C., Lin, C.-Y., Cheng, C.-H., Lai, C.-S., 2016. Spin-coated Au-nanohole arrays engineered by nanosphere lithography for a Staphylococcus aureus 16S rRNA electrochemical sensor. Biosens. Bioelectron. 77, 1086–1094.
Quarata, F., Lelli, D., Biancone, D.M., Gherardi, G., Incalzi, R.A., 2023. A urinary tract infection caused by Escherichia coli mucoid phenotype progresses to a pneumonia and respiratory failure. Lancet 401 (10380), 950.
Reta, N., Michelmore, A., Saint, C., Prieto-Simón, B., Voelcker, N.H., 2016. Porous silicon membrane-modified electrodes for label-free voltammetric detection of MS2 bacteriophage. Biosens. Bioelectron. 80, 47–53.
Reta, N., Saint, C.P., Michelmore, A., Prieto-Simon, B., Voelcker, N.H., 2018. Nanostructured electrochemical biosensors for label-free detection of water-and food-borne pathogens. ACS Appl. Mater. Interfaces 10 (7), 6055–6072.
Rogacs, A., Qu, Y., Santiago, J.G., 2012. Bacterial RNA extraction and purification from whole human blood using isotachophoresis. Anal. Chem. 84 (14), 5858–5863.
RoyChaudhuri, C., 2015. A review on porous silicon based electrochemical biosensors: beyond surface area enhancement factor. Sensor. Actuator. B Chem. 210, 310–323.
Salonen, J., Lehto, V.P., Björkqvist, M., Laine, E., Niinistö, L., 2000. Studies of thermally-carbonized porous silicon surfaces. Phys. Status Solidi 182 (1), 123–126.
Sam, S., Touahir, L., Salvador Andresa, J., Allongue, P., Chazalviel, J.-N., Gouget-Laemmel, A., Henry de Villeneuve, C., Moraillon, A., Ozanam, F., Gabouze, N., 2010. Semiquantitative study of the EDC/NHS activation of acid terminal groups at modified porous silicon surfaces. Langmuir 26 (2), 809–814.
Sciacca, B., Secret, E., Pace, S., Gonzalez, P., Geobaldo, F., Quignard, F., Cunin, F., 2011. Chitosan-functionalized porous silicon optical transducer for the detection of carboxylic acid-containing drugs in water. J. Mater. Chem. 21 (7), 2294–2302.
Seo, Y., Yoon, Y., Lee, M., Jang, M., Kim, T.-H., Kim, Y., Yoo, H.Y., Min, J., Lee, T., 2023. Rapid electrochemical biosensor composed of DNA probe/iridium nanoparticle bilayer for Aphanizomenon flos-aquae detection in fresh water. Colloids Surf. B Biointerfaces 225, 113218.
Sheng, S., Liu, L., Zhao, Z., Cai, M., Jiang, X., Kang, Y., Dai, Q., Lu, X., Xie, G., 2016. Electrochemical determination of 16s ribosomal RNA of Mycobacterium tuberculosis using magnetite on silica with DNA-functionalized gold nanoparticles. Anal. Lett. 49 (9), 1379–1387.
Shrivastava, A., Gupta, V.B., 2011. Methods for the determination of limit of detection and limit of quantitation of the analytical methods. Chronicles Young Sci. 2 (1), 21–25.
Song, K., Guo, C., Zeng, Z., Li, C., Ding, N., 2022. Factors associated with in-hospital mortality in adult sepsis with Escherichia coli infection. BMC Infect. Dis. 22 (1), 197.
Srinivasan, R., Karaoz, U., Volegova, M., MacKichan, J., Kato-Maeda, M., Miller, S., Nadarajan, R., Brodie, E.L., Lynch, S.V., 2015. Use of 16S rRNA gene for identification of a broad range of clinically relevant bacterial pathogens. PLoS One 10 (2), e0117617.
Tompkins, H.G., Irene, E.A., 2005. Handbook of Ellipsometry. William Andrew Pub, Norwich, NY. Heidelberg, Germany : Springer, Norwich, NY : Heidelberg, Germany.
Tücking, K.S., Vasani, R.B., Cavallaro, A.A., Voelcker, N.H., Schönherr, H., Prieto-Simon, B., 2018. Hyaluronic acid–modified porous silicon films for the electrochemical sensing of bacterial hyaluronidase. Macromol. Rapid Commun. 39 (19), 1800178.
Varshney, M., Mallikarjunan, K., 2009. Challenges in Biosensor Development–Detection limit, detection time, and specificity. Resour. 16 (7), 18–21.
Wang, H.-y., Kim, S., Kim, J., Park, S.-D., Uh, Y., Lee, H., 2014. Multiplex real-time PCR assay for rapid detection of methicillin-resistant staphylococci directly from positive blood cultures. J. Clin. Microbiol. 52 (6), 1911–1920.
Wang, Q., Wen, Y., Li, Y., Liang, W., Li, W., Li, Y., Wu, J., Zhu, H., Zhao, K., Zhang, J., 2019. Ultrasensitive electrochemical biosensor of bacterial 16S rRNA gene based on polyA DNA probes. Anal. Chem. 91 (14), 9277–9283.
Yang, S., Rothman, R.E., 2004. PCR-based diagnostics for infectious diseases: uses, limitations, and future applications in acute-care settings. Lancet Infect. Dis. 4 (6), 337–348.
Zou, L., Shen, R., Ling, L., Li, G., 2018. Sensitive DNA detection by polymerase chain reaction with gold nanoparticles. Anal. Chim. Acta 1038, 105–111.